applied sciences

MDPI

Article

A Novel Approach to Satellite Component Health Assessment Based on the Wasserstein Distance and Spectral Clustering

Yongchao Hui [1], Yuehua Cheng [1], Bin Jiang [1,*], Xiaodong Han [2] and Lei Yang [1]

[1] College of Automation, Nanjing University of Aeronautics and Astronautics, Nanjing 210016, China; huiyongchao@nuaa.edu.cn (Y.H.); chengyuehua@nuaa.edu.cn (Y.C.); ylsx2203154@nuaa.edu.cn (L.Y.)
[2] Communication Satellite Division, China Academy of Space Technology, Beijing 100830, China; 13426461933@163.com
* Correspondence: binjiang@nuaa.edu.cn

Abstract: This research presents a multiparameter approach to satellite component health assessment aimed at addressing the increasing demand for in-orbit satellite component health assessment. The method encompasses three key enhancements. Firstly, the utilization of the Wasserstein distance as an indicator simplifies the decision-making process for assessing the health of data distributions. This enhancement allows for a more robust handling of noisy sensor data, resulting in improved accuracy in health assessment. Secondly, the original limitation of assessing component health within the same parameter class is overcome by extending the evaluation to include multiple parameter classes. This extension leads to a more comprehensive assessment of satellite component health. Lastly, the method employs spectral clustering to determine the boundaries of different health status classes, offering an objective alternative to traditional expert-dependent approaches. By adopting this technique, the proposed method enhances the objectivity and accuracy of the health status classification. The experimental results show that the method is able to accurately describe the trends in the health status of components. Its effectiveness in real-time health assessment and monitoring of satellite components is confirmed. This research provides a valuable reference for further research on satellite component health assessment. It introduces novel and enhanced ideas and methodologies for practical applications.

Keywords: satellite components; multiparametric health assessment; Wasserstein distance; spectral clustering; seasonal decomposition

Citation: Hui, Y.; Cheng, Y.; Jiang, B.; Han, X.; Yang, L. A Novel Approach to Satellite Component Health Assessment Based on the Wasserstein Distance and Spectral Clustering. *Appl. Sci.* **2023**, *13*, 9438. https://doi.org/10.3390/app13169438

Academic Editors: Carmelo Gentile, Hanxin Chen and Qinglai Wei

Received: 4 July 2023
Revised: 27 July 2023
Accepted: 19 August 2023
Published: 21 August 2023

1. Introduction

In the field of research on satellite fault diagnosis and health management, the real-time health assessment of satellite components is a crucial task to ensure the reliability and operational stability of satellites. Conducting in-orbit health assessment studies for satellite components is significant for various purposes, including fault prediction, performance diagnosis, resource utilization, and data-driven decision making. With the development of the space industry and the increasing complexity of satellite missions, the demand for accurate assessment and real-time monitoring of satellite component health is becoming increasingly pressing [1,2]. As a result, efficient and reliable in-orbit health assessment of satellite components has become a prominent research topic.

Traditional component health assessment methods rely on expert experience and predefined rules. They also have problems such as high subjectivity and poor scalability. Meanwhile, it is difficult to establish an accurate mechanism model due to the complex structure of satellite components and the high uncertainty of space environment changes [3,4]. Therefore, accurate component health assessment by means of theoretical modeling is difficult. However, with the rapid advancement of data science and machine learning techniques, data-driven health assessment methods are gaining attention among

researchers. These methods make use of the large amount of real-time data generated by the component during operation. By analyzing and processing these data, key features are extracted. The health status of the component is assessed from a number of perspectives such as the probability of failure [5–9], remaining life [10–14], and degree of condition deviation [15,16]. Park et al. [17] obtained operational data of flywheel motors through ground-based acceleration experiments, anomaly detection, and fault prediction of satellite flywheel motors using shifted nuclear particle filters. Ibrahim et al. [18] analyzed the cause of the failure of the EgyptSat 1 satellite through a machine learning approach. A multilayer bi-directional long short-term memory (Bi-LSTM)-based fault prediction algorithm was proposed by J Gao et al. [19] to improve the prediction accuracy of intelligent algorithms. In order to avoid excessive waste of resources, Abdelghafar et al. proposed an optimized regression method based on the coyote optimization algorithm (COA) and support vector regression (SVR) to predict the remaining battery life [20]. Song et al. [21] presented an iterative update method to improve the long-term predictive performance of battery remaining life prediction. Ma et al. [22] subjected both the input-to-state and state-to-state transitions of the LSTM to convolution operations, including the temporal frequency and temporal information of the signal. This resulted in better computational efficiency and prediction accuracy when predicting the remaining life of bearing components. The classical single-parameter correlation vector regression (RVR) was extended to a multiparameter model by Wang et al. [23]. It was successfully applied to the remaining life prediction of capacitors and bearing components and good prediction results were achieved. However, due to the complexity of the orbital environment, the remaining lifetime of satellite components was strongly influenced by the random environment [24,25] and there were difficulties in the validation process. In addition, the analysis of component failure probabilities required the support of a large number of samples, while the available failure samples were very limited [26–28].

Hui et al. [15] proposed a real-time health assessment method for satellite components in orbit based on the characteristics of multiparametric data distributions. The method comprehensively considers the health of data distribution deviations (HDDDs) and the similarity of data changes (SOC). It utilizes the maximum mean difference (MMD) algorithm and Pearson correlation coefficient to describe component health status. The authors developed a multiparameter component assessment model by integrating the entropy weighting method with the criteria importance through intercriteria correlation (CRITIC) method to assign weights to parameters of the same change type. Additionally, the empirical modal decomposition (EMD) technique was employed for trend extraction and comparative validation. This method requires a small amount of sample data and is easy to validate. Good results have been achieved in all tests using a large amount of real satellite component operational data. However, the method has a few shortcomings. Firstly, the original method is only applicable to the multiparameter fusion assessment of the same type of parameters of a component, restricting its application to the comprehensive assessment of combinations of different types of parameters. Secondly, the determination of threshold values still relies on expert experience and lacks objectivity and updating. In summary, the method provides a new idea and approach for satellite component health assessment. However, further research and improvement are still needed to improve its applicability and accuracy.

Building upon previous research, this research proposes an improved and optimized method to address the above limitations. (1) The improved Wasserstein distance (WD) is introduced as an alternative measure to HDDD and SOC calculations. This optimization simplifies the decision-making process for assessing the results and provides a more accurate description of changes in the health status of satellite components. Additionally, the method is extended to accommodate the assessment of multiple types of parameters, surpassing the original approach, which only evaluates single parameter types. (2) Spectral clustering is used to determine the boundaries of different health status classes to replace traditional methods that rely on expert experience. By using spectral clustering, the health

states of satellite components can be automatically classified. This also provides a more scientific, objective, and reliable means of assessment and enhances the accuracy and repeatability of the assessment method.

The experimental results confirm the capability of the newly proposed method to accurately capture the evolving trends in the health status of satellite components. Its effectiveness in the real-time assessment and monitoring of satellite component health is validated. The next sections describe, in detail, the optimization method presented in this research and the experimental results to demonstrate its potential for application in the field of satellite component health assessment.

2. Problem Description and Overall Program

2.1. Problem Description

This research aims to optimize the original method to address two specific challenges, with the goal of providing a more versatile approach to component health assessment.

First, the MMD mentioned in [15] is capable of describing departures in the data distribution. However, it solely focuses on overall differences and fails to consider variations in the location distributions. Therefore, it needs to be complemented with Pearson coefficients to capture the similarities of data changes (SOC). The challenge lies in effectively combining both indicators when making decisions regarding assessment results. Additionally, different mapping functions are chosen for different types of data variations. This restricts the original method to being suitable only for the multiparameter fusion evaluation of the same type of parameters within a component. For instance, the original method can only select current data exhibiting the same type of variation across the four axes of a gyro. Another example is temperature data demonstrating the same type of variation on a solar sail. Figure 1a illustrates the current data for the four axes of a gyro, indicating that they vary in precisely the same manner. In contrast, Figure 1b depicts the bearing temperature and current data for a momentum wheel, revealing that they do not exhibit the same type of variation.

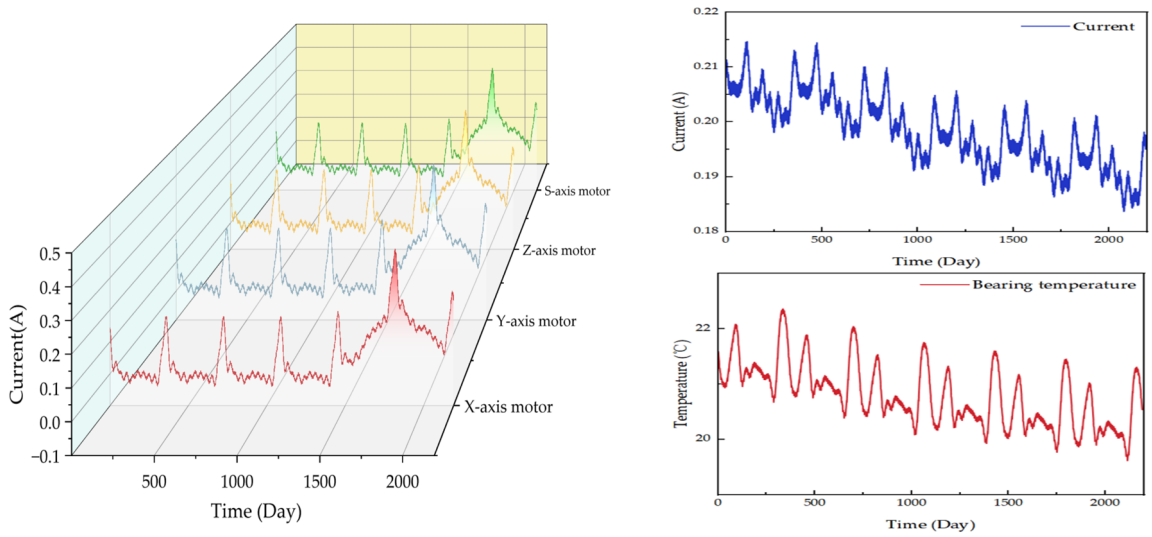

(**a**) Gyroscope (**b**) Momentum wheel

Figure 1. Variation in health characteristic parameters of different components.

Figure 2 shows the results of the MMD calculations for two sets of data with different types of changes. The second set of data in each graph is obtained by adding one to the first set of data magnitudes, with no other changes. However, the MMD results obtained at this point in the calculation are different. In short, the calculated MMD results are not the same

when different variation types of parameters have the same degree of data distribution deviation (DDD).

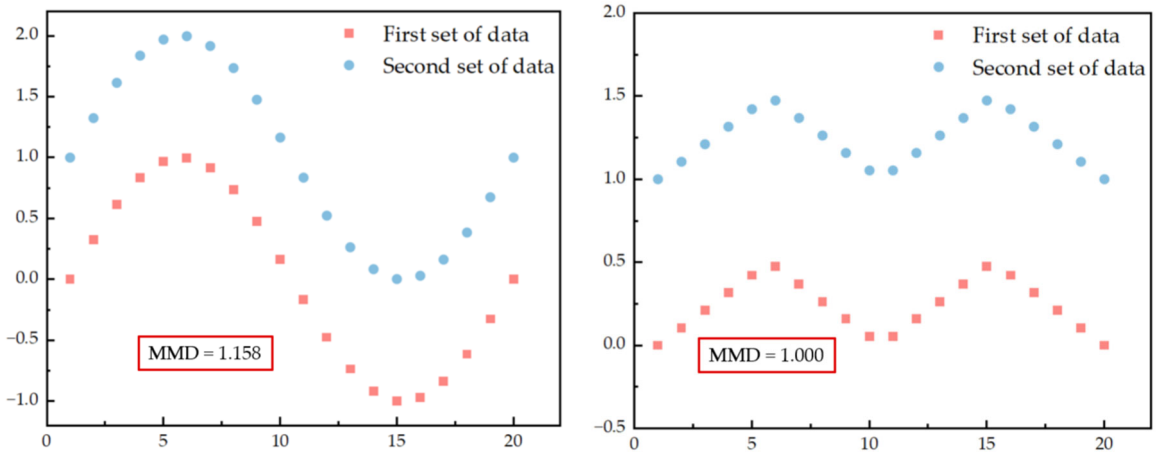

(**a**) First type of data change (**b**) Second type of data change

Figure 2. Effectiveness of MMD calculations for data with different change types.

Considering the need to combine different types of parameters for a more comprehensive component health assessment, another consideration is to simplify the decision-making process for the assessment results. This research introduces the WD as a proxy indicator to describe the differences in the data distribution and to provide more comprehensive, accurate, and interpretable assessment results [29,30].

Second, the determination of health status thresholds for satellite components traditionally relies on expert experience. However, expert experience is highly subjective, difficult to update, and may not fully leverage the potential information present in the data. To overcome these limitations, this research introduces a spectral clustering approach to determine threshold values. Spectral clustering is a nonparametric clustering method that does not require assumptions to be made about the data distribution. It is applicable to various types of data, including health status monitoring data of satellite components. Spectral clustering has the advantages of adapting to complex data structures, taking into account global information, scalability, and the absence of prelabeled samples [31]. It enables a more scientific, accurate, and reasonable classification of component health status.

2.2. Overall Program

The method presented in this research comprises three main stages: assessment modeling, online assessment, and validity verification. The overall program of the method is shown in Figure 3.

(1) In the assessment modeling phase, the component historical telemetry data are first preprocessed. The benchmark range is determined using metrics such as variance and standard deviation. From this, the healthiness assessment indicator for the component's whole-life data, i.e., HDDD, is calculated. Simultaneously, the whole-life data are employed to assign appropriate weights to individual parameters. Subsequently, the health status classes are classified based on the spectral clustering method and reasonable thresholds are determined for the subsequent online assessment.

(2) In the online assessment phase, health benchmark state data are first collected and used to build a benchmark model of the component. Once the benchmark data collection is complete, the real-time component health assessment commences. During the real-time assessment process, the health status indicator of the component is calculated using the improved Wasserstein distance (WD). The results of the HDDD calculation are then compared with predefined thresholds to determine the corresponding health status level of the component.

(3) In the validity verification phase, trends in the long-term data are extracted using the seasonal decomposition (SD) algorithm. These trends extracted through SD are analyzed and compared to the results obtained from the HDDD based on the WD. Comparative analyses are used to verify the effectiveness of the method in capturing trends in component health status changes.

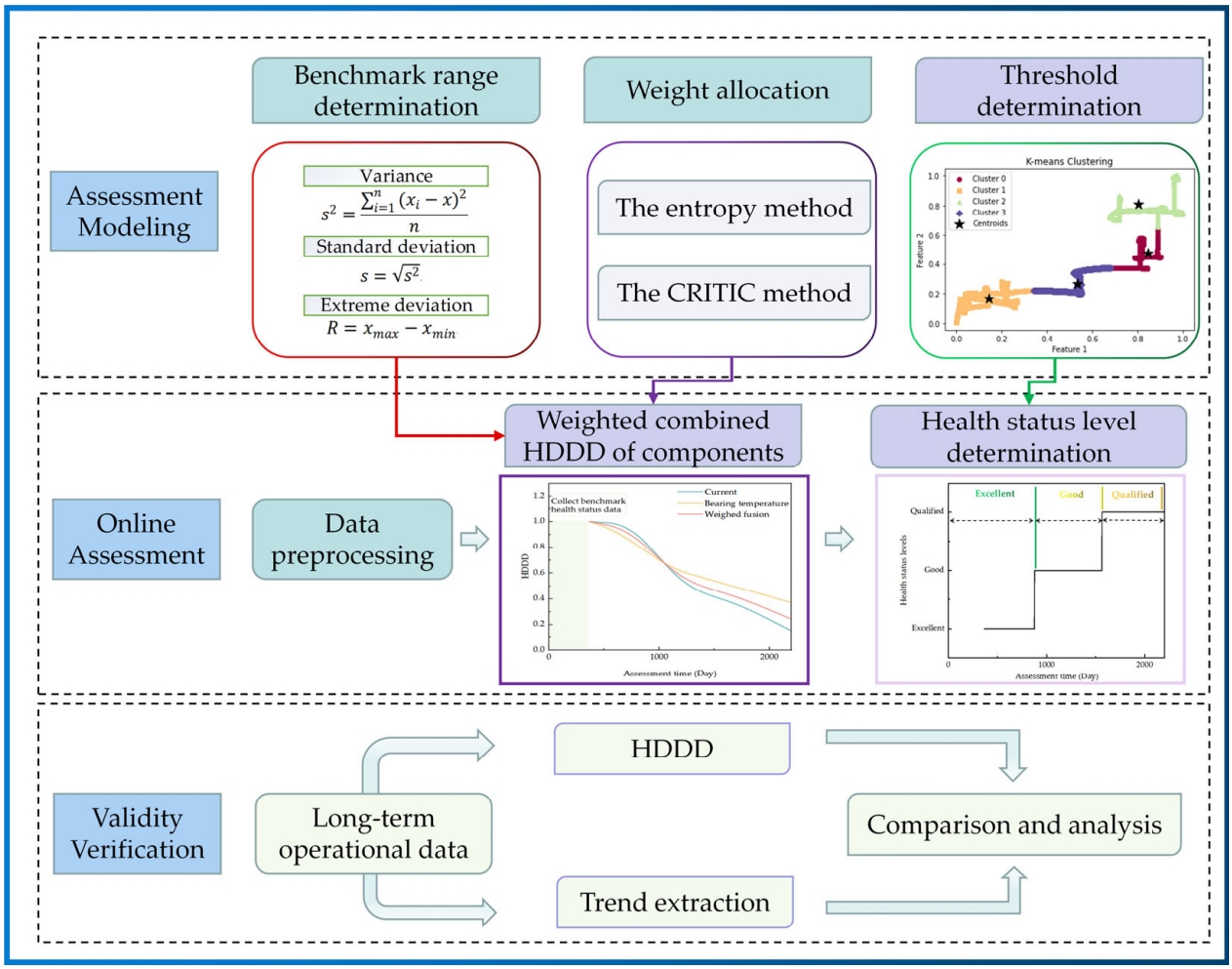

Figure 3. Overall program.

3. Program Design

3.1. WD-Based Multiparameter Component Assessment Model

3.1.1. WD-Based Single Parameter Health Calculation

Among the commonly used methods to characterize the differences in data distributions are total variation, JS dispersion, KL distance, etc. However, for satellite data with complex variations, the Wasserstein distance is more suitable than these methods. Total variation is insensitive to subtle variations in the distribution and shape differences, which makes it difficult to capture early anomalies in components in time [32]. JS dispersion does not accurately reflect the differences in dealing with nonoverlapping data distributions. The asymmetric characteristics of the KL distance make its results unstable [33].

To overcome these limitations, the Wasserstein distance (WD) is introduced as a mathematical tool for measuring differences in probability distributions. It has attracted a lot of attention and research in recent years with the rise of deep learning. The WD was proposed to address some of the limitations and shortcomings of the traditional distance metric when dealing with probability distributions [29,34]. It provides more information when measuring differences between data, rather than being limited to statistical distributions of

values. In contrast to the MMD, the WD takes into account the differences in position and shape between the two distributions. It captures nonlinear relationships and local nuances, assessing the dissimilarity by determining the optimal mass transfer between distributions. The WD quantifies the average cost of transporting mass from one distribution to another in an optimal manner [34–36]. In summary, the superiority of the WD lies in its ability to take into account the structure and shape of probability distributions. The WD describes the differences between the state distributions of data by minimizing the transfer cost. This gives it better performance in dealing with practical problems such as multimodality, high-dimensional data, and noise and makes it more suitable compared with other distribution description methods [37].

The mathematical representation of the WD is as follows [30,38]:

$$\mathrm{Wp}\ (\mathrm{P},\mathrm{Q}) = \left(\inf_{\gamma \in \pi(\mathrm{P},\mathrm{Q})} \int_{\mathrm{R}\ \times\ \mathrm{R}} ||\mathrm{x}\ -\ \mathrm{y}\ ||^{\mathrm{p}} \mathrm{d}\gamma\ (\mathrm{x},\mathrm{y}) \right)^{\frac{1}{\mathrm{p}}} \tag{1}$$

where π(P,Q) denotes the set of all joint probability distributions with marginal distributions P and Q; γ is the transfer plan from P to Q, which describes how the mass is transferred from P to Q.

In the component assessment model, the WD is used to describe the variability between the real-time operational data of the component and the benchmark data. By calculating the WD, a positive data distribution health indicator, HDDD, can be obtained to quantify the health status of the component.

$$\mathrm{HDDD}\ =\ 1\ -\ \mathrm{W_p}(\mathrm{P},\mathrm{Q}) \tag{2}$$

A high HDDD value indicates a small difference between the real-time data and the benchmark data, suggesting that the component is in a good state of health. Conversely, a low HDDD value indicates a potential abnormality or deterioration in the component's health.

The advantage of the new method is illustrated by the X-axis current data of a faulty gyroscope. The data are derived from telemetry data from a real satellite. From Figure 4, it can be seen that the current data are abnormally elevated around day 1500 and a fault occurs. At this time, both the SOC and HDDD based on the WD capture the anomaly timely and accurately. However, the HDDD based on the MMD is not sensitive to the anomaly and has a certain lag. This reflects the ability of the HDDD based on the WD to detect faults and anomalies in a timely manner, especially in the early stages of faults and anomalies. The temporary increase in the similarity of current data around day 2050 causes the SOC results to be temporarily unavailable, which needs to be considered together with the HDDD based on the MMD to ensure that no erroneous results occur. Therefore, the method proposed in reference [15] needs to consider these two indicators at the same time. These two indicators complement each other in performing a reasonable and complete component health assessment. However, the HDDD based on the WD approach does not suffer from these two problems. Using only one HDDD based on the WD indicator, the health status of each component can be assessed in a timely, accurate, and comprehensive manner. Thus, the new method solves the problem of the difficulty in rationally integrating multiple indicators for decision making.

The WD has several important advantages over traditional distance metrics. Firstly, the WD can handle nonoverlapping or partially overlapping distributions, which traditional methods often struggle with. This allows for more comprehensive comparisons in various scenarios. Secondly, the WD has better robustness to outliers and noise and can better accommodate anomalies in real data [39,40]. Most importantly, the WD has better interpretability compared with the results of the MMD and can more accurately describe the degree of deviation from the component state.

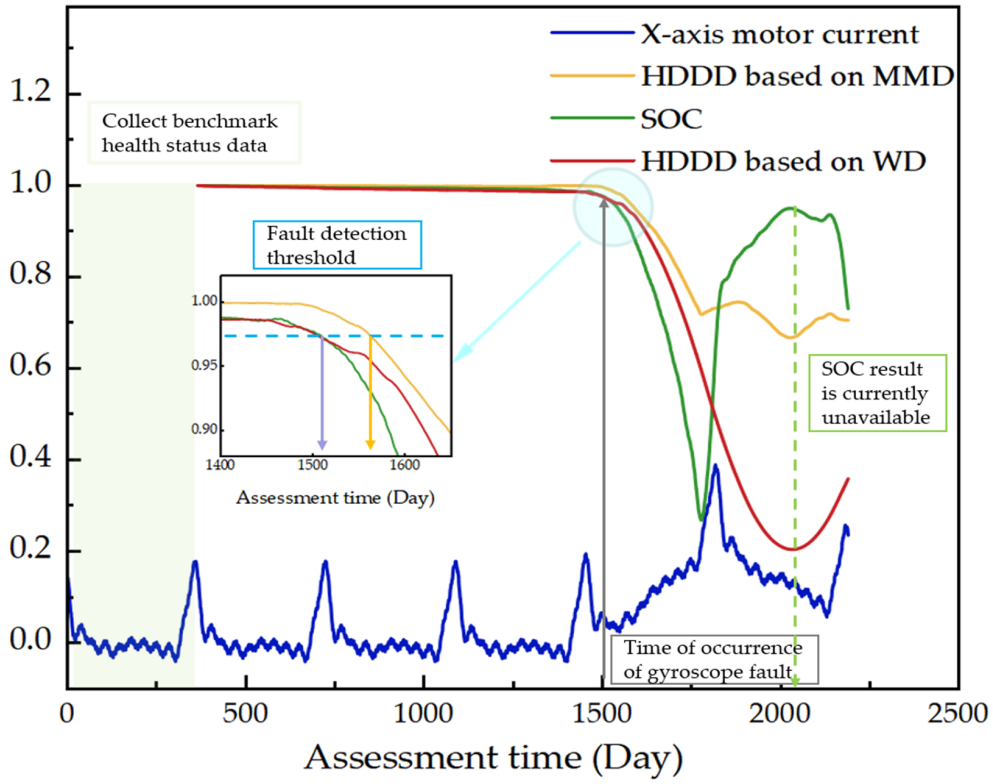

Figure 4. Comparison of the effectiveness of different single-parameter health state description methods.

3.1.2. Multiparametric Assessment Models Based on Data Standardization

Since different types of parameters exhibit significant differences in amplitude and variation, direct calculation of their HDDD and weighted fusion is not feasible. Therefore, there is a need to make improvements to the WD-based HDDD calculation method. First, the benchmark data for the parameters are normalized. Then, the mapping process is performed on the real-time operational data using the extreme values of the benchmark data so that parameters of different variation types are on the same scale. Next, HDDDs of different parameters can then be compared and fused. In this way, the problem of difficulty in reasonably fusing the results of multiple categories of parameters due to different types of amplitude and parameter variation can be solved.

After the benchmark data have been collected, the benchmark data for the different parameters first need to be normalized in the forward direction. Assume that the data of the parameter ζ_i are $[x_1, \cdots, x_m, \cdots, x_n, \cdots]$ and the corresponding benchmark data are $[x_1, \cdots, x_m]$, where the maximum value is $\zeta_i^h(\max)$ and the minimum value is $\zeta_i^h(\min)$. The formula for the forward normalization of the benchmark data is:

$$y_i = \frac{x_i - \zeta_i^h(\min)}{\zeta_i^h(\max) - \zeta_i^h(\min)} \ (1 \le i \le m) \tag{3}$$

Subsequent data are mapped according to the changes in the benchmark data. The mapping method is shown in Equation (4):

$$y_n = \frac{x_n - \zeta_i^h(\min)}{\zeta_i^h(\max) - \zeta_i^h(\min)} \ (n > m) \tag{4}$$

After the mapping process, the degree of deviation of the different variation types of parameters can be calculated and reasonably fused according to the method presented in this research. Taking the shell temperature data of a solar sail component of a star as an example, the effect after the above operation is shown in Figure 5.

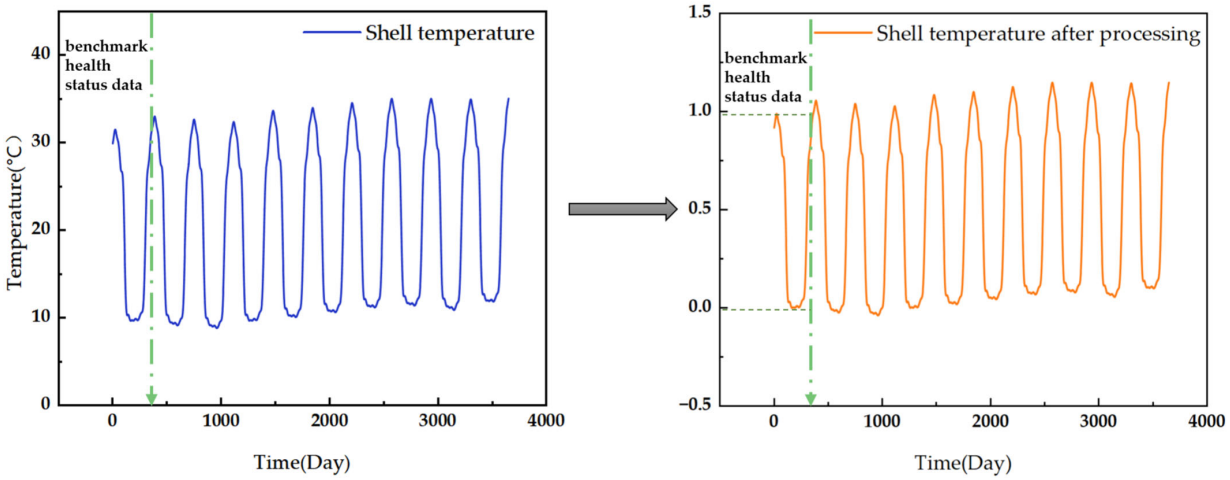

Figure 5. Data standardization and mapping effects.

By combining the entropy and CRITIC methods, a comprehensive component assessment model is established. The average value of the weights calculated using the two methods is taken as the final weight of the parameters. This model takes into account multiple parameters and their respective weights, providing a holistic evaluation of the health status of the component. The fusion process ensures that the assessment results are based on the collective information from all relevant parameters, leading to a more accurate and reliable assessment outcome. In Equation (5), ξ_i is the ith health feature parameter of the component, w_i is the weight of the ith health feature parameter, and $f(\xi_i)$ is the HDDD of the ith health feature parameter.

$$f(\xi) = w_1 f(\xi_1) + w_2 f(\xi_2) + \cdots + w_n f(\xi_n) \quad (5)$$

3.2. Classification of Health Status Classes Based on Spectral Clustering

Due to the limitations of expert experience, which is subjective, limited, and difficult to update, it is difficult to determine reasonable thresholds to classify health states for different components. For satellite components in particular, the status of a component can often only be classified as "qualified" or "failed" by means of a fixed threshold. This inevitably leads to a waste of satellite resources.

Spectral clustering is a nonparametric clustering method that groups data based on graph theory and linear algebraic methods [41]. Compared with traditional clustering methods, spectral clustering focuses more on the relationship and similarity between samples rather than relying only on the distance between samples. In the classification of component health status levels, there may be complex intrinsic connections and interactions between samples; spectral clustering can better capture these relationships to more accurately classify health status levels. Additionally, spectral clustering has the following unique advantages: (1) it is suitable for nonconvex data distributions and can accurately capture complex structures and correlations; (2) it has strong robustness and is effective in handling noise and outliers and the clustering results are not easily distorted [42,43]; (3) the number of states can be divided artificially to adapt to different situations.

When using spectral clustering for health status ranking, the WD-based HDDD is used as a feature. The main calculation steps are as follows [44]:

① Construct a similarity matrix S, where S(i, j) denotes the similarity of the ith data point to the jth data point.

② Construct the Laplace matrix. The Laplace matrix L is constructed from the similarity matrix S. The commonly used Laplace matrices are the standard Laplace matrix and the symmetric normalized Laplace matrix. The standard Laplace matrix is defined as

$$L = D - S \quad (6)$$

where D is the degree matrix and the diagonal elements represent the degree of each data point. The symmetric normalized Laplace matrix is defined as

$$L = I - D^{-1/2}SD^{-1/2} \tag{7}$$

where I is the unit matrix.

③ Eigenvector decomposition. Eigenvector decomposition is performed on the Laplace matrix L to obtain the eigenvectors and the corresponding eigenvalues.

$$Lv = \lambda v \tag{8}$$

where L is the Laplace matrix, v is the eigenvector, and λ is the eigenvalue. The eigenvector corresponding to the first k eigenvalues is usually chosen as the new data representation, where k is the specified number of clusters.

④ Clustering. The data are clustered using a clustering algorithm (e.g., K means) based on the information in the feature vector. The data are classified into different classes of health status.

We present an example using the solar sail shell temperature and bearing temperature data from a real satellite. As there are generally no "failure" states, except for severe failures and end of life, the HDDD of the ten-year data was therefore clustered into three states: "Excellent, Good and Qualified". The original data and the HDDD clustering effect are shown in Figure 6.

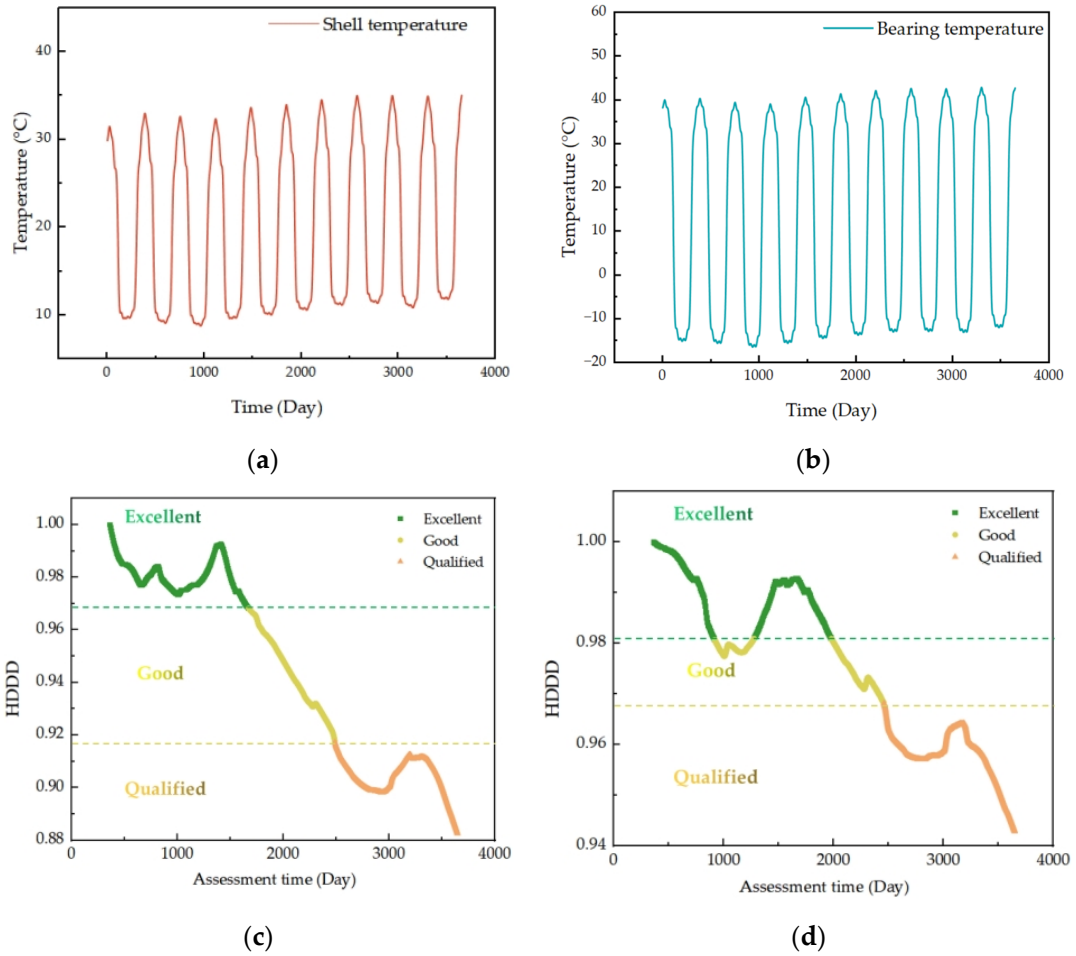

Figure 6. The HDDD for the (**a**) shell temperature and (**b**) bearing temperature of a solar sail. (**c**) The spectral clustering effect of HDDD for shell temperature. (**d**) The spectral clustering effect of HDDD for bearing temperature.

Figure 6 clearly demonstrates that, even for the same degree of degradation, different health characteristic parameters of the same component yield varying HDDD values. Therefore, the health state thresholds should be different for different components. It can be observed that the different state classes in Figure 6 are clearly delineated and clustered well. However, the use of expert experience only allows for delineation using fixed thresholds. It is difficult to take into account the differences in different parametric data characteristics and component types. In summary, spectral clustering is scientifically valid and effective in classifying component health status classes. By considering the characteristics and similarities of the data, the health status classes of components can be classified more accurately. This also provides a useful reference for subsequent health condition monitoring and maintenance.

It is important to note that the application of this method presupposes the availability of complete lifetime history data for this type of component. This allows for spectral clustering and the determination of reasonable thresholds.

3.3. Verification of Validity Based on Seasonal Decomposition

For long-term data on the stable operation of components, the use of empirical modal decomposition (EMD), while capable of extracting accurate trends, suffers from two shortcomings. Firstly, the influence of unknown factors, such as the orbital environment, can lead to data embodying health that is not ideally monotonically decreasing. When performing nonmonotonic trend extraction, a suitable modal function (e.g., IMF) needs to be selected for decomposition based on experience or expert knowledge. This involves subjective judgement and parameter selection, which can lead to subjective bias in the results for complex variation data. Secondly, EMD is highly sensitive to data specificity. When anomalies with nonsmooth, nonlinear, or noisy data are encountered, EMD may produce inaccurate or unstable results [45,46].

In contrast, the seasonal decomposition (SD) algorithm is widely used in time series analysis and offers distinct advantages. It decomposes time series data into three components: seasonal, trend, and stochastic. Compared with EMD, SD has the advantages of deterministic decomposition, targeting periodic data, providing trend analysis, and handling periodic noise [47,48]. At the same time, SD does not require human selection of modal functions or adjustment of parameters. Subjectivity and human intervention are avoided, providing more consistent and repeatable results. This makes it very suitable when dealing with data with fixed periodic variations, such as satellite component data. It is based on the principle of analyzing periodic and trend changes in time series and decomposing the data into components of different frequencies [49].

SD can be expressed in Equation (9):

$$Y(t) = T(t) + S(t) + R(t) \tag{9}$$

where Y(t) represents the time series data, T(t) represents the trend component, S(t) represents the seasonal component, and R(t) represents the stochastic component.

The main steps of the algorithm are as follows:

① First, the trend component is estimated using smoothing techniques (e.g., moving averages):

$$T(t) = f(T(t)) \tag{10}$$

② Next, the trend component is subtracted from the raw data to obtain the detrended data:

$$Y'(t) = Y(t) - T(t) \tag{11}$$

③ The data are then detrended by calculating the cyclical variation at each point in time. The seasonal component is estimated:

$$S(t) = g(Y'(t)\Big) \tag{12}$$

④ Finally, the seasonal component is subtracted from the detrended data to obtain the remaining stochastic component:

$$R(t) = Y'(t) - S(t) \tag{13}$$

Through such a decomposition process, the time series data can be split into three components: trend, seasonality, and stochastic. Analysis of the data and trend extraction are achieved.

The advantages of this method are illustrated in particular in reaction flywheel case temperature data that appear to be anomalous. As can be seen in Figure 7, the shell temperature data for this component are complex and, at the same time, anomalous at around day 1200. EMD for such data can only extract the trend of late rising changes through global description. This is not fully consistent with the real data trend; however, the characteristics of SD make it possible to extract an accurate trend of change for these data. The fact that accurate descriptions can also be generated in detail illustrates the strength of this method.

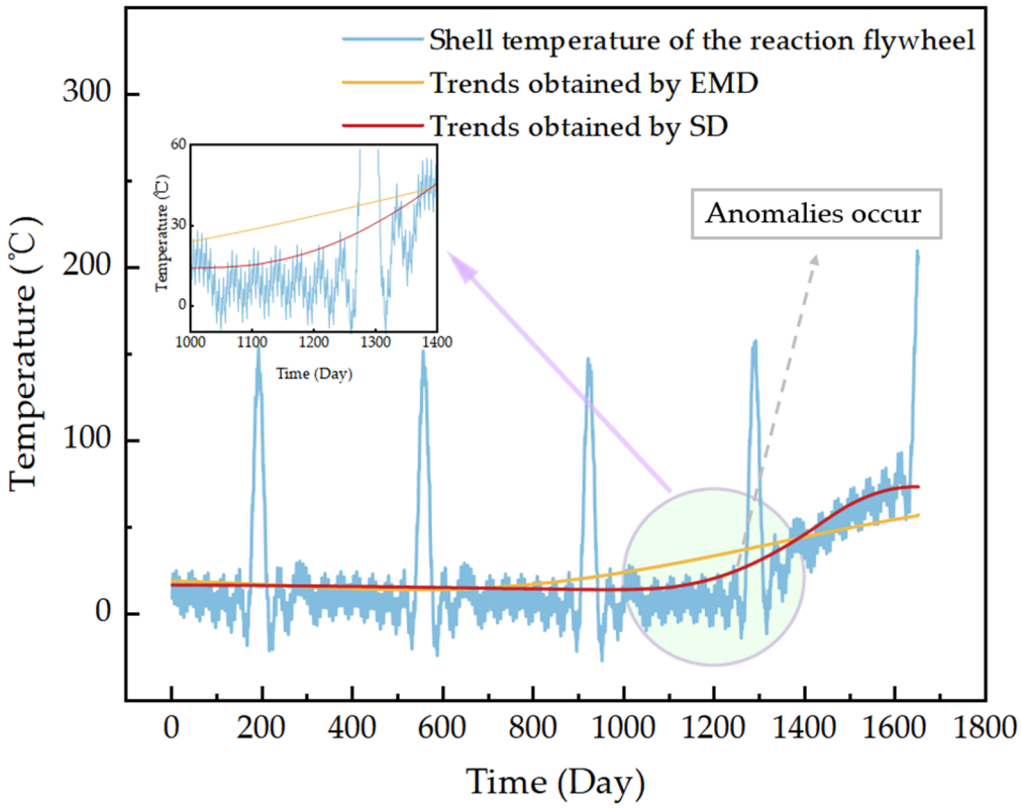

Figure 7. Comparison of trend extraction methods.

4. Experiment and Verification

The validity of the method is illustrated in Section 3 using data such as the gyroscope current under failure and the full-life temperature of a solar sail. In this research, we focus on the different types of variations in component health characteristic parameters. To provide a more comprehensive illustration, we present a complete case study using operational data from a real satellite's momentum wheels.

4.1. Component Assessment Modeling

The momentum wheel is a key actuating component of the satellite attitude control system. It regulates the speed and direction by controlling the current. Changes in the current parameter have a direct impact on the performance of the momentum wheel.

Therefore, if the current parameter is unstable or too large or too small, it may lead to an unstable rotational speed of the momentum wheel, increased attitude control errors, or failure to achieve the required attitude adjustment. At the same time, abnormal changes in temperature parameters can indirectly affect the performance of the momentum wheel by influencing the friction characteristics, inertia characteristics, and motor performance. In a closed-loop satellite attitude control system, monitoring and control of temperature are very important to ensure the proper operation and accurate attitude adjustment of the momentum wheel. Based on the above considerations, the bearing temperature and current of a momentum wheel component are selected. Seven years of whole-life data are used to assess and analyze the validity of the methodology presented in this study. Figure 8 shows the original data for these two health characteristics after preprocessing with wild-value rejection and resampling.

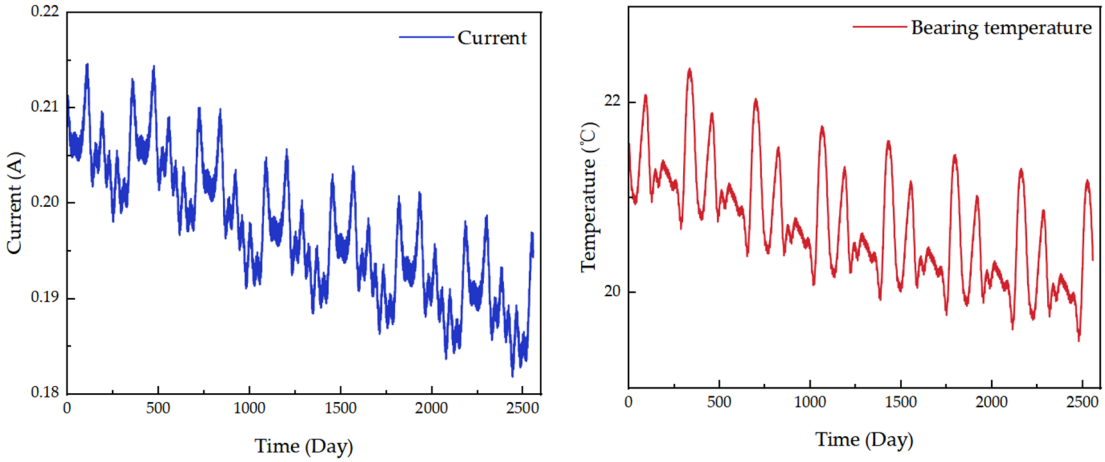

Figure 8. The current (**a**) and bearing temperature (**b**) data of the momentum wheel after preprocessing.

As can be seen in Figure 8, the current data are extremely stable for the first two years, with no significant changes in amplitude. Around day 700, there is significant performance degradation, with a decreasing trend in the current amplitude. The temperature data show a relatively gentle downward trend overall.

Using the first cycle data as the health state benchmark, the two parameters are normalized positively. The results are shown in Figure 9. The weights are calculated using the entropy weighting method and CRITIC method; the mean value is taken as the combined weight. The results are shown in Table 1. The details of the method can be found in [15] and will not be repeated here.

Table 1. Results of the calculation of the parameter weights.

	Weighting of Current	Weighting of Bearing Temperature
CRITIC method	0.512	0.488
Entropy method	0.486	0.514
Combined weighting	0.499	0.501

The combined weight of the current was 0.499 and the combined weight of the bearing temperature is 0.501. The assessment model for the momentum wheel component is shown in Equation (14):

$$f(\xi) = 0.499f(\xi_1) + 0.501f(\xi_2) \quad (14)$$

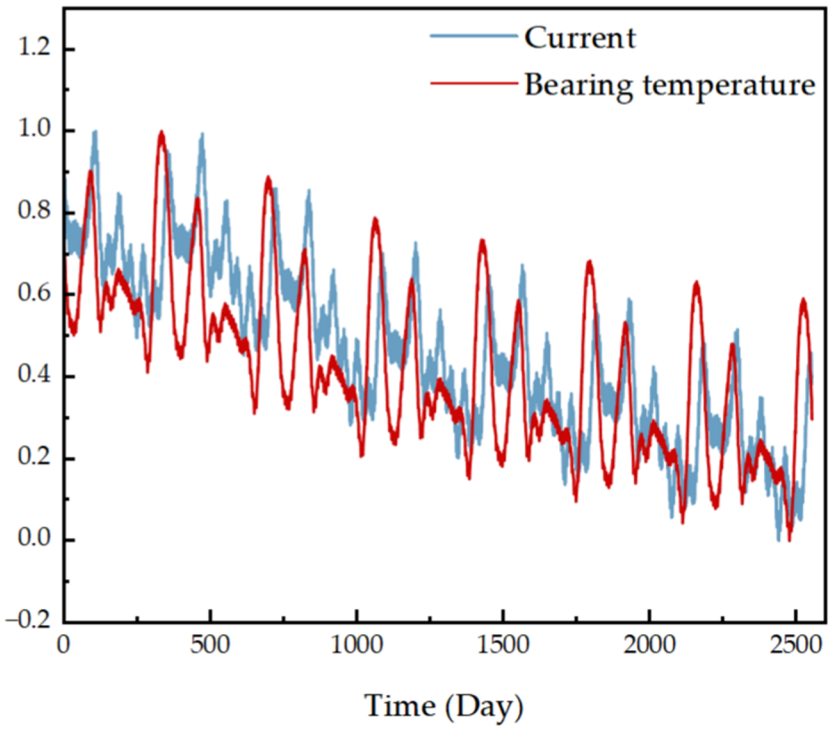

Figure 9. Positive normalization of the current and bearing temperature.

4.2. Component Health Assessment

The health indicator HDDD is calculated separately for the two parameters. The results of the two parameters are then weighted and fused using the assessment model. The results are shown in Figure 10.

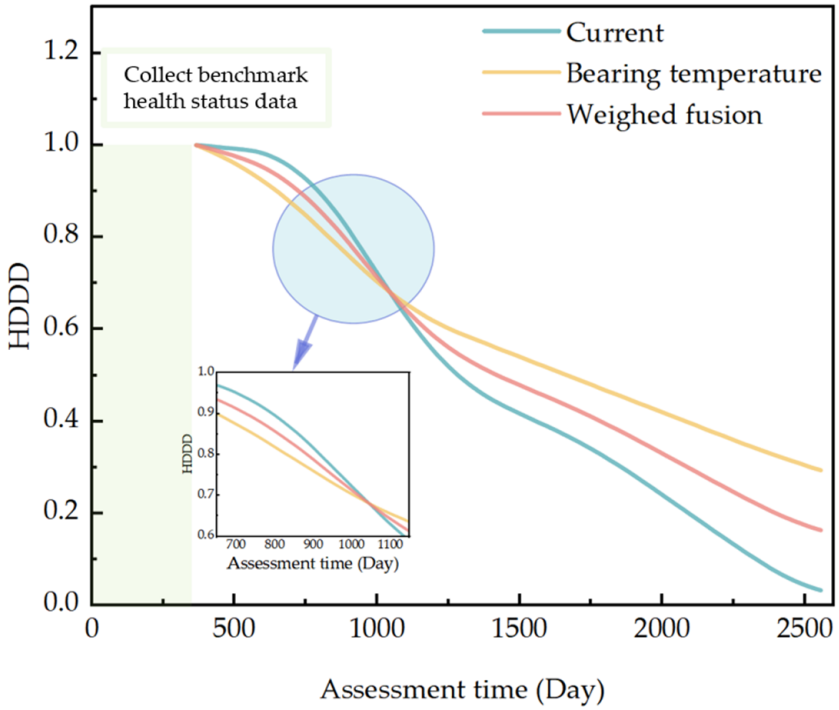

Figure 10. The results of the calculation of the component health indicator HDDD.

During the initial phase of the orbital run, the HDDD of the current data shows minimal changes, while the HDDD of the temperature data exhibits a significant downward trend. Starting from approximately day 700, there is a rapid decline in the health of the current data, surpassing the rate of decline in the temperature data. After day 1050, the health of the current data falls below that of the bearing temperature parameter. These changes align well with the original data and the method accurately describes the variations in health for both parameters, demonstrating its validity.

As these data are for the full life of the momentum wheel component in stable operation, the component is not in a state of complete "failure". Therefore, the health status of the component has gone through three levels: excellent, good, and qualified. The combined HDDD of the momentum wheel component is used as a feature and the health status classes are classified using spectral clustering. The results of the threshold classification are presented in Table 2.

Table 2. Results of threshold calculation.

	Excellent	Good
HDDD	0.821	0.338

Based on the thresholds, the curve for the change in the health status of the momentum wheel component is shown in Figure 11.

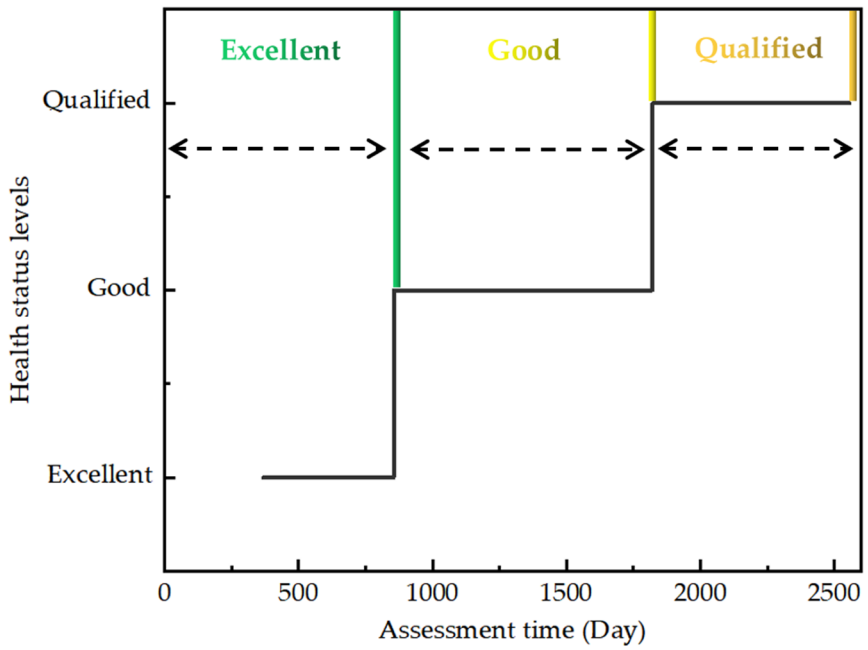

Figure 11. Chart of component health status level changes.

Figure 11 clearly demonstrates the rapid degradation of the component's performance, reaching a passable condition within approximately five years. Despite this degradation, the component is still capable of performing certain work tasks. By conducting real-time in-orbit health assessments of key components, it becomes possible to strategically allocate work tasks based on the component's status. This approach effectively prevents unnecessary waste of satellite resources.

4.3. Verification of Validity

Long-term data trends in the current and bearing temperature are extracted using SD. The results are shown in Figure 12.

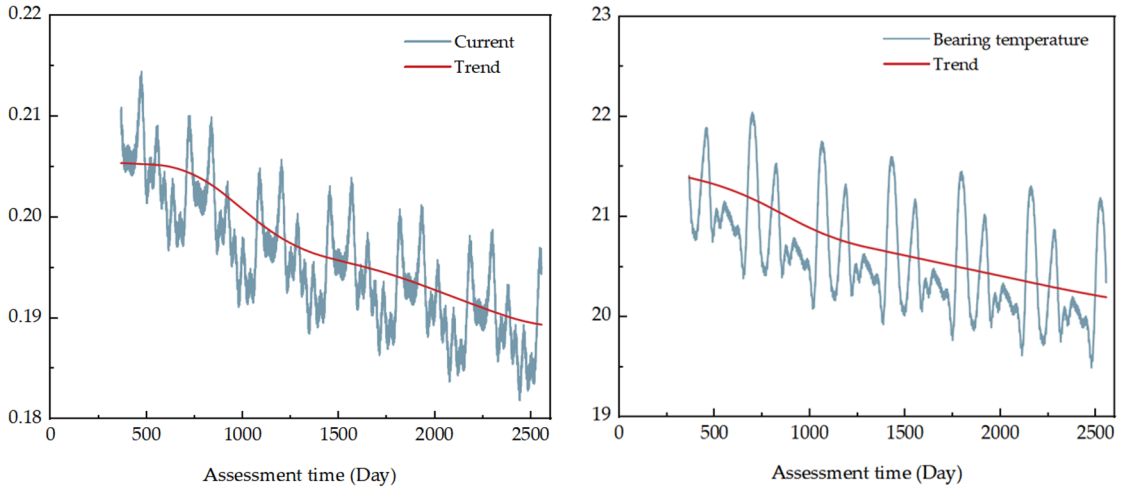

(**a**) Current (**b**) Bearing temperature

Figure 12. Trend extraction based on the seasonal decomposition algorithm.

The long-term trends in the current and bearing temperature are normalized positively to the HDDD variation curve. A comparison of the normalized trends is shown in Figure 13. The similarity between the two sets of trends is evaluated using three measures: Pearson correlation coefficient, root mean square error (RMSE), and mean absolute error (MAE). The results of these calculations are summarized in Table 3.

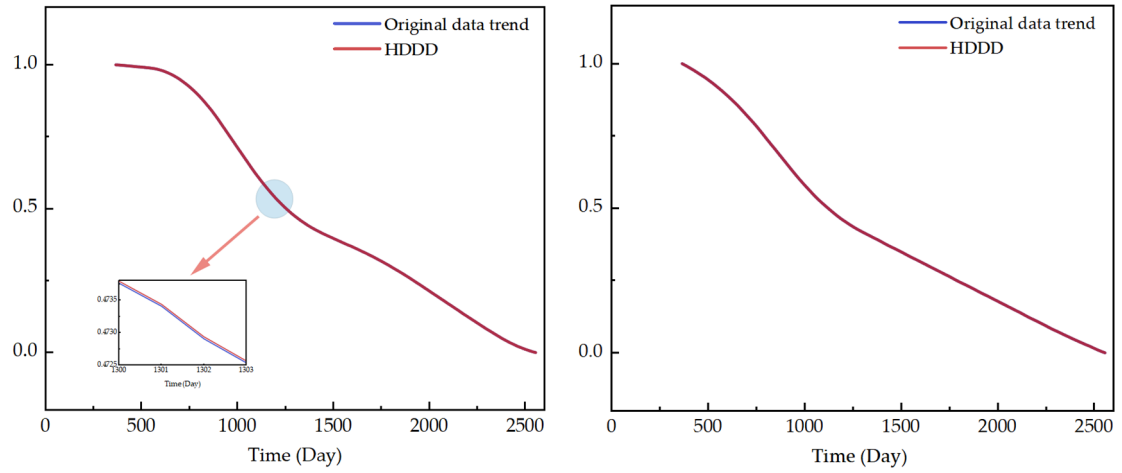

(**a**) (**b**)

Figure 13. Comparison of the two trends in the (**a**) current and (**b**) bearing temperature after positive normalization.

Table 3. Calculation of trend change similarity indicators.

Indicator	Current	Bearing Temperature
Pearson correlation coefficient	0.999	0.999
RMSE	3.622×10^{-5}	3.273×10^{-5}
MAE	2.986×10^{-5}	2.652×10^{-5}

As can be observed from the calculations in Figure 13, there is a very high similarity between the trends in the complete long-term data extracted using SD and the trends in the HDDD based on the WD. Although slight variations can be observed in certain details, the

magnitudes of the RMSE and MAE, as presented in Table 3, are all on the order of 10^{-4}. The consistency of the change is also reflected in the results of the similarity metrics. The method presented in this research relies on a single indicator for the description of health changes. However, SD first generates model assumptions and parameter estimates for the overall data and then extracts accurate trends by processing the long-term data. The validation results, which indicate a high degree of similarity, fully demonstrate the validity and accuracy of the method.

5. Conclusions

In this research, an optimized multiparameter satellite component health assessment method based on the Wasserstein distance and spectral clustering is presented. This method offers four advantages over the original method [15] (which only relies on short-term data for accurate in-orbit health assessment): (1) The HDDD is calculated based on the improved WD. Compared with methods such as the MMD and JS dispersion, the WD can provide more comprehensive, accurate, and interpretable assessment results. At the same time, it solves the challenge of rational and comprehensive decision making with multiple indicators. (2) By preprocessing the benchmark standardization of different change types of parameters, the fusion of multiple parameters of the same variation type in the original method is extended to the fusion of multiple parameters of different variation types. This makes the fusion process more scientific and rational. (3) A spectral clustering algorithm is used to determine the boundaries of health status classes, avoiding the subjectivity when relying on expert experience while adapting to the clustering needs of different types of data. (4) The use of the seasonal decomposition algorithm to extract trends in nonmonotonic health state changes enhances the accuracy of the validation of the assessment results. This improves the validation of the assessment results for different data scenarios.

Through these improvements, this research complements and refines the original method in terms of theory, application, and validation. The combination of the two methods enables an accurate description of the real-time health status of components under stable operation, faults, abnormalities, and backup switching. This research provides a valuable reference in the field of in-orbit health assessment of key satellite components. It also provides guidance for further application of the assessment method to components in other systems. Future research will continue to build on this foundation to expand the application of the assessment method to more systems.

Author Contributions: Conceptualization, Y.H., Y.C. and B.J.; methodology, Y.H.; validation, Y.H., X.H. and Y.C.; formal analysis, Y.H.; investigation, Y.H. and Y.C.; data curation, Y.H. and L.Y.; writing—original draft preparation, Y.H. and Y.C.; writing—review and editing, Y.H. and B.J. All authors have read and agreed to the published version of the manuscript.

Funding: This research was funded by the National Natural Science Foundation Integration Project (No. U22B6001) and the Nanjing University of Aeronautics and Astronautics Forward-Looking Research Project (No. ILA22041).

Institutional Review Board Statement: Not applicable.

Informed Consent Statement: Not applicable.

Data Availability Statement: The data used for the example in this paper are the actual in-orbit operational data from a satellite after processing, which are private information and therefore not disclosed here.

Acknowledgments: The authors of this paper would like to thank the FDD team at Nanjing University of Aeronautics and Astronautics for their support in this research. We also thank the editors for their rigorous and efficient work and the reviewers for their helpful suggestions.

Conflicts of Interest: The authors declare no conflict of interest.

References

1. Tao, L.; Zhang, T.; Peng, D.; Hao, J.; Jia, Y.; Lu, C.; Ding, Y.; Ma, L. Long-term degradation prediction and assessment with heteroscedasticity telemetry data based on GRU-GARCH and MD hybrid method: An application for satellite. *Aerosp. Sci. Technol.* **2021**, *115*, 106826. [CrossRef]
2. Zhang, B.; Wu, Y.; Zhao, B.; Chanussot, J.; Hong, D.; Yao, J.; Gao, L. Progress and challenges in intelligent remote sensing satellite systems. *IEEE J. Sel. Top. Appl. Earth Obs. Remote Sens.* **2022**, *15*, 1814–1822. [CrossRef]
3. Vichard, L.; Steiner, N.Y.; Zerhouni, N.; Hissel, D. Hybrid fuel cell system degradation modeling methods: A comprehensive review. *J. Power Sources* **2021**, *506*, 230071. [CrossRef]
4. Rui, K.; Wenjun, G.; Yunxia, C. Model-driven degradation modeling approaches: Investigation and review. *Chin. J. Aeronaut.* **2020**, *33*, 1137–1153.
5. Zhang, K.; Jiang, B.; Yan, X.-G.; Mao, Z. Incipient fault detection for traction motors of high-speed railways using an interval sliding mode observer. *IEEE Trans. Intell. Transp. Syst.* **2018**, *20*, 2703–2714. [CrossRef]
6. Liu, J.; Tang, Q.; Qiu, W.; Ma, J.; Duan, J. Probability-based failure evaluation for power measuring equipment. *Energies* **2021**, *14*, 3632. [CrossRef]
7. Xiao, N.-C.; Yuan, K.; Zhou, C. Adaptive kriging-based efficient reliability method for structural systems with multiple failure modes and mixed variables. *Comput. Methods Appl. Mech. Eng.* **2020**, *359*, 112649. [CrossRef]
8. Lee, I.; Lee, U.; Ramu, P.; Yadav, D.; Bayrak, G.; Acar, E. Small failure probability: Principles, progress and perspectives. *Struct. Multidiscip. Optim.* **2022**, *65*, 326. [CrossRef]
9. Liu, Q.; Wang, C.; Wang, Q. Bayesian Uncertainty Inferencing for Fault Diagnosis of Intelligent Instruments in IoT Systems. *Appl. Sci.* **2023**, *13*, 5380. [CrossRef]
10. Yuehua, C.; Liang, J.; Bin, J.; Ningyun, L. Useful life prediction using a stochastic hybrid automata model for an ACS multi-gyro subsystem. *J. Syst. Eng. Electron.* **2019**, *30*, 154–166.
11. Strzelecki, P. Determination of fatigue life for low probability of failure for different stress levels using 3-parameter Weibull distribution. *Int. J. Fatigue* **2021**, *145*, 106080. [CrossRef]
12. Chen, Y.; Peng, G.; Zhu, Z.; Li, S. A novel deep learning method based on attention mechanism for bearing remaining useful life prediction. *Appl. Soft Comput.* **2020**, *86*, 105919. [CrossRef]
13. Chen, Z.; Wu, M.; Zhao, R.; Guretno, F.; Yan, R.; Li, X. Machine remaining useful life prediction via an attention-based deep learning approach. *IEEE Trans. Ind. Electron.* **2020**, *68*, 2521–2531. [CrossRef]
14. Wang, M.; Wang, H.; Cui, L.; Xiang, G.; Han, X.; Zhang, Q.; Chen, J. Remaining Useful Life Prediction for Aero-Engines Based on Time-Series Decomposition Modeling and Similarity Comparisons. *Aerospace* **2022**, *9*, 609. [CrossRef]
15. Hui, Y.; Cheng, Y.; Jiang, B.; Yang, L. A Method for Satellite Component Health Assessment Based on Multiparametric Data Distribution Characteristics. *Aerospace* **2023**, *10*, 356. [CrossRef]
16. Schwabacher, M. A survey of data-driven prognostics. In Proceedings of the Infotech@ Aerospace, Arlington, Virginia, 26–29 September 2005; p. 7002.
17. Park, H.J.; Kim, S.; Lee, J.; Kim, N.H.; Choi, J.-H. System-level prognostics approach for failure prediction of reaction wheel motor in satellites. *Adv. Space Res.* **2023**, *71*, 2691–2701. [CrossRef]
18. Ibrahim, S.K.; Ahmed, A.; Zeidan, M.A.E.; Ziedan, I.E. Machine learning techniques for satellite fault diagnosis. *Ain Shams Eng. J.* **2020**, *11*, 45–56. [CrossRef]
19. Gao, J.; Wang, H.; Shen, H. Task failure prediction in cloud data centers using deep learning. *IEEE Trans. Serv. Comput.* **2020**, *15*, 1411–1422. [CrossRef]
20. Abdelghafar, S.; Goda, E.; Darwish, A.; Hassanien, A.E. Satellite lithium-ion battery remaining useful life estimation by coyote optimization algorithm. In Proceedings of the 2019 Ninth International Conference on Intelligent Computing and Information Systems (ICICIS), Cairo, Egypt, 8–10 December 2019; pp. 124–129.
21. Yuchen, S.; Datong, L.; Yandong, H.; Jinxiang, Y.; Yu, P. Satellite lithium-ion battery remaining useful life estimation with an iterative updated RVM fused with the KF algorithm. *Chin. J. Aeronaut.* **2018**, *31*, 31–40.
22. Ma, M.; Mao, Z. Deep-convolution-based LSTM network for remaining useful life prediction. *IEEE Trans. Ind. Inform.* **2020**, *17*, 1658–1667. [CrossRef]
23. Wang, X.; Jiang, B.; Wu, S.; Lu, N.; Ding, S.X. Multivariate relevance vector regression based degradation modeling and remaining useful life prediction. *IEEE Trans. Ind. Electron.* **2021**, *69*, 9514–9523. [CrossRef]
24. Pardini, C.; Anselmo, L. Environmental sustainability of large satellite constellations in low earth orbit. *Acta Astronaut.* **2020**, *170*, 27–36. [CrossRef]
25. Boudjemai, A.; Hocine, R.; Guerionne, S. Space environment effect on earth observation satellite instruments. In Proceedings of the 2015 7th International Conference on Recent Advances in Space Technologies (RAST), Istanbul, Turkey, 16–19 June 2015; pp. 627–634.
26. Chen, H.; Jiang, B.; Ding, S.X.; Lu, N.; Chen, W. Probability-relevant incipient fault detection and diagnosis methodology with applications to electric drive systems. *IEEE Trans. Control Syst. Technol.* **2018**, *27*, 2766–2773. [CrossRef]
27. Zhou, C.; Xiao, N.-C.; Zuo, M.J.; Gao, W. An improved Kriging-based approach for system reliability analysis with multiple failure modes. *Eng. Comput.* **2022**, *38*, 1813–1833. [CrossRef]

28. Wang, X.; Shen, C.; Xia, M.; Wang, D.; Zhu, J.; Zhu, Z. Multi-scale deep intra-class transfer learning for bearing fault diagnosis. *Reliab. Eng. Syst. Saf.* **2020**, *202*, 107050. [CrossRef]
29. Rüschendorf, L. The Wasserstein distance and approximation theorems. *Probab. Theory Relat. Fields* **1985**, *70*, 117–129. [CrossRef]
30. Panaretos, V.M.; Zemel, Y. Statistical aspects of Wasserstein distances. *Annu. Rev. Stat. Its Appl.* **2019**, *6*, 405–431. [CrossRef]
31. Von Luxburg, U. A tutorial on spectral clustering. *Stat. Comput.* **2007**, *17*, 395–416. [CrossRef]
32. Chambolle, A. An algorithm for total variation minimization and applications. *J. Math. Imaging Vis.* **2004**, *20*, 89–97.
33. Nielsen, F. On a generalization of the Jensen–Shannon divergence and the Jensen–Shannon centroid. *Entropy* **2020**, *22*, 221. [CrossRef]
34. Chen, Y.; Ye, J.; Li, J. Aggregated Wasserstein distance and state registration for hidden Markov models. *IEEE Trans. Pattern Anal. Mach. Intell.* **2019**, *42*, 2133–2147. [CrossRef] [PubMed]
35. Hoshino, K. Finite-horizon control of nonlinear discrete-time systems with terminal cost of Wasserstein distance. In Proceedings of the 2020 59th IEEE Conference on Decision and Control (CDC), Jeju Island, Republic of Korea, 14–18 December 2020; pp. 4268–4274.
36. Zhao, G.; Cai, Z.; Wang, X.; Dang, X. GAN Data Augmentation Methods in Rock Classification. *Appl. Sci.* **2023**, *13*, 5316. [CrossRef]
37. Xu, C.; Wang, J.; Yang, W.; Yu, H.; Yu, L.; Xia, G.-S. Detecting tiny objects in aerial images: A normalized Wasserstein distance and a new benchmark. *ISPRS J. Photogramm. Remote Sens.* **2022**, *190*, 79–93. [CrossRef]
38. Peyré, G.; Cuturi, M. Computational optimal transport: With applications to data science. *Found. Trends®Mach. Learn.* **2019**, *11*, 355–607. [CrossRef]
39. Leo, J.; Ge, E.; Li, S. Wasserstein Distance in Deep Learning. Available online: https://papers.ssrn.com/sol3/papers.cfm?abstract_id=4368733 (accessed on 18 August 2023).
40. Sun, H.; Yang, Z.; Cai, Q.; Wei, G.; Mo, Z. An extended Exp-TODIM method for multiple attribute decision making based on the Z-Wasserstein distance. *Expert Syst. Appl.* **2023**, *214*, 119114. [CrossRef]
41. Kang, Z.; Shi, G.; Huang, S.; Chen, W.; Pu, X.; Zhou, J.T.; Xu, Z. Multi-graph fusion for multi-view spectral clustering. *Knowl.-Based Syst.* **2020**, *189*, 105102. [CrossRef]
42. Huang, D.; Wang, C.-D.; Wu, J.-S.; Lai, J.-H.; Kwoh, C.-K. Ultra-scalable spectral clustering and ensemble clustering. *IEEE Trans. Knowl. Data Eng.* **2019**, *32*, 1212–1226. [CrossRef]
43. Sun, G.; Cong, Y.; Dong, J.; Liu, Y.; Ding, Z.; Yu, H. What and how: Generalized lifelong spectral clustering via dual memory. *IEEE Trans. Pattern Anal. Mach. Intell.* **2021**, *44*, 3895–3908. [CrossRef]
44. Verma, D.; Meila, M. A comparison of spectral clustering algorithms. *Univ. Wash. Tech. Rep. UWCSE030501* **2003**, *1*, 1–18.
45. Lin, J.; Dou, C.; Liu, Y. Multifractal detrended fluctuation analysis based on optimized empirical mode decomposition for complex signal analysis. *Nonlinear Dyn.* **2021**, *103*, 2461–2474. [CrossRef]
46. Yang, Y.; Wang, J. Forecasting wavelet neural hybrid network with financial ensemble empirical mode decomposition and MCID evaluation. *Expert Syst. Appl.* **2021**, *166*, 114097. [CrossRef]
47. Wen, K.; Zhao, G.; He, B.; Ma, J.; Zhang, H. A decomposition-based forecasting method with transfer learning for railway short-term passenger flow in holidays. *Expert Syst. Appl.* **2022**, *189*, 116102. [CrossRef]
48. Apaydin, H.; Sattari, M.T.; Falsafian, K.; Prasad, R. Artificial intelligence modelling integrated with Singular Spectral analysis and Seasonal-Trend decomposition using Loess approaches for streamflow predictions. *J. Hydrol.* **2021**, *600*, 126506. [CrossRef]
49. Gao, J.; Song, X.; Wen, Q.; Wang, P.; Sun, L.; Xu, H. Robusttad: Robust time series anomaly detection via decomposition and convolutional neural networks. *arXiv* **2020**, arXiv:2002.09545.